AFM Visualization of Individual and Periodic Assemblies of a Helical Dendronized Polyphenylacetylene on Graphite

Virgil Percec,*,† Jonathan G. Rudick,† Martin Wagner,† Makoto Obata,† Catherine M. Mitchell,† Wook-Dong Cho,† and Sergei N. Magonov‡

Roy & Diana Vagelos Laboratories, Department of Chemistry, University of Pennsylvania, Philadelphia, Pennsylvania 19104-6323, and Digital Instruments, Veeco Metrology Group, Santa Barbara, California 93117-3107

Received April 14, 2006; Revised Manuscript Received August 8, 2006

ABSTRACT: Self-organization of individual dendronized poly(phenylacetylene) (PPA) macromolecules on highly oriented pyrolytic graphite (HOPG) is revealed by atomic force microscopy (AFM). The dendronized PPA is composed of amphiphilic, self-assembling dendrons. Individual macromolecules are imaged as oblate cylindrical objects whose relative orientation in the first layer adsorbed to the HOPG reflects underlying lattice symmetry. This is due to epitaxial adsorption of the peripheral alkyl tails. Thermal annealing results in large domains of uniformly oriented dendronized PPAs (i.e., 2D nematic order) due to intermolecular interactions. Periodicity within domains and between layers is dictated by the height and width of the oblate cylindrical PPA. A further consequence of epitaxy is that at the HOPG interface the PPA backbone adopts a more extended conformation than the helical cis−cisoidal conformation of the internally ordered hexagonal columnar (Φ_h^{io}) phase found in bulk. Well-ordered domains of cylindrical helical dendronized PPAs offer the potential to exploit single-handed helical chirality at the HOPG surface.

Introduction

Self-assembly of organic molecules on various substrates, which arises from the interplay of intermolecular, intramolecular, and interfacial interactions, attracts considerable interest from researchers who are developing new biomaterials, functional coatings, supramolecular electronics, supramolecular chirality sensors, and other nanostructured functional materials.[1] Characterization of organic layers on substrates has been substantially improved with the introduction of scanning tunneling microscopy (STM) and atomic force microscopy (AFM).[2] Both methods provide high-resolution imaging of surface structures. Consequently, visualization of single molecules and their organization within surface layers has become an efficient procedure for surface structural analysis.[3]

Initially, STM was applied to study molecular order at the liquid−solid interface, and the images of alkylcyanobiphenyls,[4] normal alkanes (C_nH_{2n+1}),[5] and cyclic alkanes (C_nH_{2n})[6] deposited on highly oriented pyrolytic graphite (HOPG) have revealed an epitaxial order of these adsorbates. The epitaxy is governed by alignment of extended alkane chains along the main lattice directions of the substrate.[7] In addition, there is a tumbling of alkane molecules between two different orientations of its all-trans conformation: the zigzag backbone either lies flat or is oriented perpendicular with respect of the substrate surface. This has been noticed in STM images[8] and a study using neutron scattering.[9]

Imaging individual synthetic macromolecules has become a significant focus to bring about better understanding of macromolecular structure and conformation on substrates as well as their self-assembled motifs. Such imaging has been demonstrated on single-layer assemblies of polystyrene-*b*-poly(methyl methacrylate) prepared by the Langmuir−Blodgett technique on water and transferred onto mica.[10] These applications were further extended to visualization of liquid crystalline dendrimers,[11] cylindrically shaped macromolecular brushes,[12] and dendronized polymers.[13−17] AFM Images revealed individual polymers as isolated species as well as in flat arrays and layers on various substrates (e.g., mica, HOPG, or Si wafer). Recent advances in synthesis have provided a number of novel macromolecules with fine-tuned chemical structure and low polydispersity.[14,15,18] For characterization of these polymers, AFM assists GPC, light scattering, electron microscopy, and X-ray diffraction (XRD).

In contrast to ordinary chain macromolecules, chains of brush[12] and dendronized[13−17] polymers experience steric repulsions due to densely grafted side chains. Consequently, these chains adopt an extended conformation, and in AFM images they are seen as wormlike objects of several nanometers in diameter. It is remarkable that macromolecules with self-assembling dendrons as side groups exhibit preferential orientation along surface lattice directions of HOPG. Such epitaxy helps unravel the macromolecules on the substrate and ensures their mechanical stability with respect to the tip force in AFM experiments. Most of the AFM studies of polymers with self-assembling dendritic groups[13] have been carried out with relatively large macromolecules (M_w = 40−100 kDa) whose contour length varies in the 100−150 nm range. It is rather important to learn if shorter macromolecules with a smaller number of alkyl groups interacting with HOPG can be examined with AFM. Lamellae consisting of tens of single poly(oxazoline) macromolecules with tapered dendritic side groups (degree of polymerization, DP = 500), which adopt a completely extended conformation, have been clearly seen in AFM images.[14] An average length of these macromolecules, which are well resolved in the lamellae blocks, is around 23 nm. Yet isolated macromolecules have been seen only occasionally. AFM images of the poly(oxazolines) with DP = 100 show crystalline-like assemblies of these macromolecules arising from their end-to-end self-assembly.[14] Again,

† University of Pennsylvania.
‡ Digital Instruments.
* Corresponding author. E-mail: percec@sas.upenn.edu.

10.1021/ma060845g CCC: $33.50
Published on Web 09/21/2006

Scheme 1

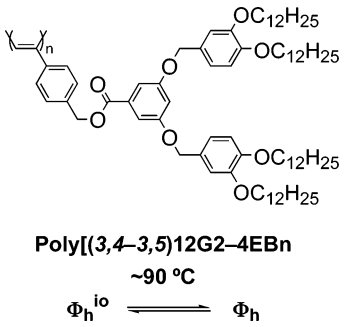

Poly[(*3,4–3,5*)12G2–4EBn

~90 °C

$\Phi_h^{io} \rightleftharpoons \Phi_h$

isolated macromolecules with low DP have not been clearly identified.

Poly(phenylacetylene)s (PPAs) are considered to be dynamic helical polymers whose handedness can be selected by a chiral, nonracemic environment.[19] Initial efforts to visualize synthetic helical PPAs on a substrate by STM were complicated by structural changes in the polymer.[20a] This is likely the result of electrocyclization and oxidative chain cleavage of the polyene backbone, as has been shown to occur by thermal treatment in solution and in bulk.[21] AFM visualization of helical PPAs has shown that superhelical aggregates are the most common feature.[20] Uniform monolayers and films with helical structure have not yet been visualized.

We have applied AFM for visualization of poly[(*3,4*−*3,5*)-12G2−4EBn] and its self-assemblies on HOPG (Scheme 1). The results of this study, which are presented below, reveal a rodlike conformation of this macromolecule in a layer immediately lying on HOPG. This order does not exist in the top layers. Within the first adsorbed layer, there is a strong tendency to form liquid crystalline order on different scales depending on the polymer thermal history.

Results

Macromolecular Arrays. Samples were prepared by spin-casting from THF solution. Surface coverage varied according to the solution concentration. When a shortage of material does not allow a complete coverage of the substrate even with a single layer, we have observed arrays of macromolecules scattered over the HOPG surface (Figure 1). These arrays are composed of rodlike and grain structures, which are 0.5−0.9 nm in height. These estimates were obtained after examining a number of height images, which were recorded at different tip−sample forces. Most likely, the top value is closer to a true vertical size of poly[(*3,4*−*3,5*)12G2−4EBn] macromolecules adsorbed on graphite. A tip-induced deformation is responsible for low height values of the macromolecular arrays. Streaky patches occasionally observed during imaging of this sample (cf. ones indicated with the arrows in Figure 1a) indicate a disturbance of the macromolecules by the AFM probe. Remarkable features, which are seen in both images, are rodlike structures packed in small domains that are surrounded by grains and a less-ordered material. These rods are oriented along directions coinciding with the hexagonal symmetry of the graphite lattice. Such epitaxy is common for ordering of polymer molecules with self-assembling dendritic groups.[13e,14] The length of the rods is ~24 nm.

The assemblies of single macromolecules, which are described above, have been observed in poly[(*3,4*−*3,5*)12G2−4EBn] samples after spin-casting or dipping without any thermal annealing. Thermal annealing of another sample with low-coverage of the surface produced a very different morphology.

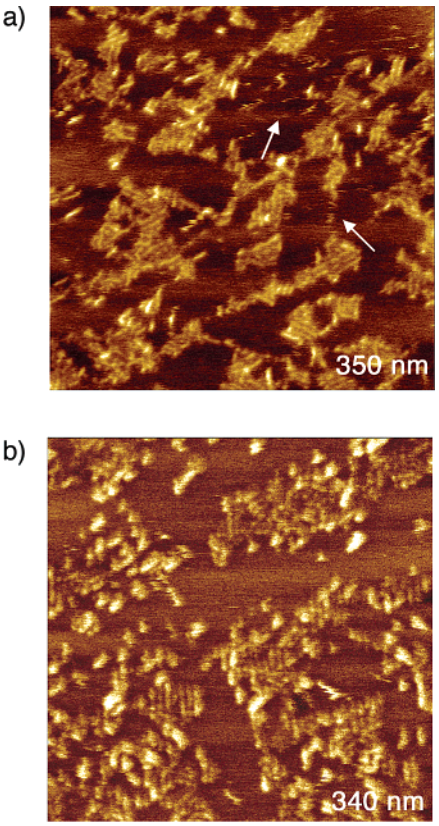

Figure 1. AFM images of poly[(*3,4*−*3,5*)12G2−4EBn] macromolecules deposited on HOPG by (a) spin-casting (phase image; arrows indicate locations where macromolecules are damaged by the probe) and (b) dipping (height image). The samples were examined without any thermal annealing.

In this case, polymer droplets and single-layer domains are seen in the height and phase images (Figure 2). Apparently, uniform wetting and spreading do not take place on poorly covered surfaces. This is in contrast to the ordered domains described below for highly covered surfaces. The droplets, which have an onion shape with a height up to 40 nm, resemble those seen in earlier AFM images of carbosilane dendrimers.[11b,c] Ringlike features of different contrast, which are seen in the phase images, indicate that a macromolecular ordering within these droplets is rather heterogeneous. The wetting angle of these droplets, which was estimated from the droplet profile, was ~5°. The single-layer domains of different lateral size are most pronounced in the phase images. The height of these domains evaluated from the height image obtained in light tapping is ~0.7 nm. With increasing force the apparent height becomes smaller (i.e., 0.5 nm). The high-magnification images obtained in hard tapping show that these layers are composed of individual rods, which can be assigned to individual macromolecules or their assemblies. A small domain, which is seen between the droplets (Figure 2c), consists primarily of two lamellae of extended poly[(*3,4*−*3,5*)12G2−4EBn] macromolecules emphasized by three dotted lines. A part of this domain is shown in the high-resolution image in Figure 2d. The bright rods inside this domain are ~23 nm in length and ~4 nm in width. A separation between neighboring rods is ~7 nm.

Figure 3a shows a large domain consisting of blocks with different orientation of the macromolecular rods. Such directional order, emphasized by white lines in the image, is consistent with the symmetry of the underlying HOPG. Most of the rods are aligned along two directions as seen in the FFT power spectrum in the left top corner of this image. At the

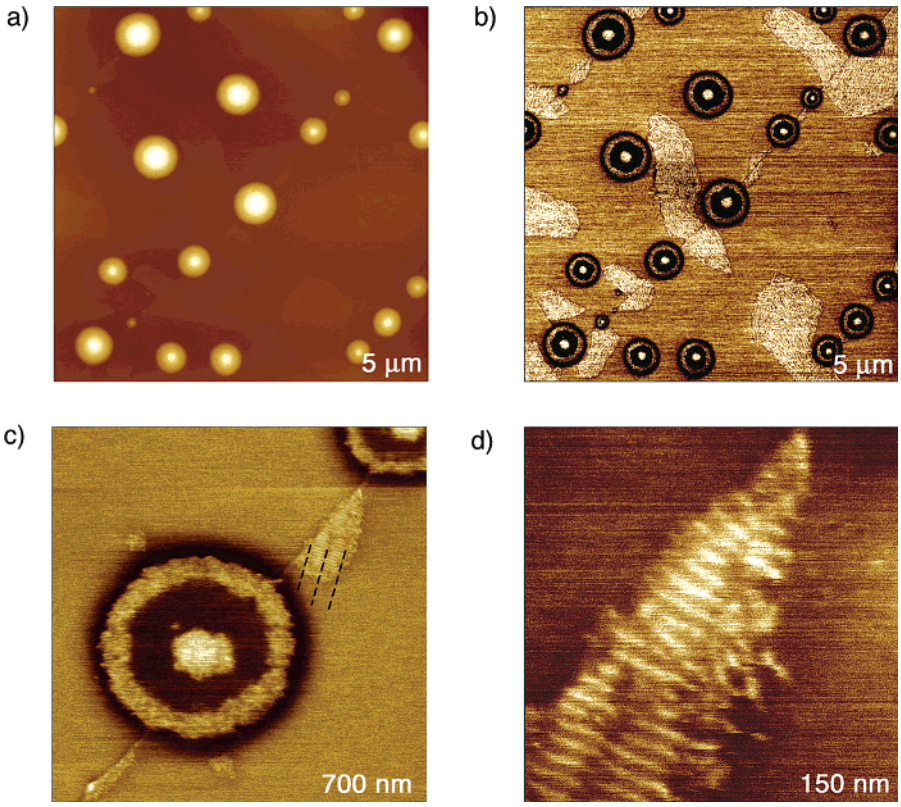

Figure 2. AFM (a) height and (b−d) phase images of a poly[(*3,4*−*3,5*)12G2−4EBn] sample with low coverage of the substrate after annealing at 100 °C for 1 h. (c) Magnification of a selected region in (b), wherein the black dotted lines indicate macromolecular lamella structures of a single layer domain. (d) Magnification of the single layer domain shown in (c).

interface between the domains with different orientations (Figure 3b), one sees a tendency of the rods to form extended linear structures (30−50 nm in length). In some locations, one can identify individual lamellar blocks (e.g., those marked 1 and 2 in Figure 3b) with an average width ∼25 nm. The observed self-assembly of poly[(*3,4*−*3,5*)12G2−4EBn] in this domain indicates that, in addition to epitaxy of these macromolecules to the HOPG, there is a competition between the intermolecular interactions involving side and terminal groups of neighboring extended macromolecules. The hydrophobic interactions between side groups promote the formation of the lamellae and those between the terminal groups generate a long-range linear order.

It is worth noting that individual rods are best resolved at elevated tip−sample forces. In light tapping, only corrugated surface features are seen in the height image (Figure 4a), while the phase image (Figure 4b) is almost featureless. Both images change with increasing force (Figure 4c,d), and individual rods became partially seen in the phase image (Figure 4d). Ultimately, both height and phase images show well-resolved rods similar to those seen in Figure 3. The transition from light tapping to hard tapping was accompanied by a small (∼0.2 nm) change in height. We suggest that a thin poorly ordered overlayer either of peripheral alkyl tails or a contaminant covered the single layer. The increased tip−sample force penetrates such a soft overlayer without disturbing the conformation of the dendronized PPA.

Single Layers. The previously reported[15] DSC results were kept in mind while examining poly[(*3,4*−*3,5*)12G2−4EBn] samples, which have been obtained by spin-casting. A phase transition occurs at ∼90 °C, which has been shown to relate to the reversible transition from a hexagonal columnar lattice with internal columnar order (Φ_h^{io}) to a normal hexagonal columnar (Φ_h) lattice at higher temperature (Scheme 1). Though thermal behavior of poly[(*3,4*−*3,5*)12G2−4EBn] in thin layers on HOPG might be different than in bulk, we have followed structural changes in poly[(*3,4*−*3,5*)12G2−4EBn] samples being annealed at 50 and 100 °C. The stability of poly(arylacetylene)s in bulk and solution is a concern because of thermally induced 6π electrocyclization along the polymer backbone and oxidative chain cleavage.[21] We have shown that poly[(*3,4*−*3,5*)12G2−4EBn] is thermally stable for the thermal treatments described herein.[15a]

Figure 5a shows the AFM phase image of a surface region completely covered by a single layer of poly[(*3,4*−*3,5*)12G2−4EBn] macromolecules. It is characterized by an interwoven pattern formed of numerous rods of 4−5 nm in width and 30−50 nm in length. The rods are oriented along three main directions (hexagonal symmetry) as indicated by FFT power spectrum in the inset. After annealing at 50 °C for 1 h, the structure of this layer underwent distinctive changes related to the formation of submicron domains with different orientation of elongated linear structures, which are composed of smaller rods (Figure 5b). Further annealing of the sample at 100 °C led to the increase of the domain size and improvement of macromolecular ordering within the domains (Figure 5c). An averaged distance between the macromolecular rods and their elongated assemblies has been determined from power spectrum density analysis of the high-magnification AFM images of these structures (Figure 6). An average distance between the macromolecular rods in the spin-cast sample prior to the thermal annealing is estimated as 8.5 nm. The spacing between the macromolecules of the annealed samples varies from one domain to another. The densest macromolecular packing with a spacing of 7.2 nm was observed within one of the most ordered domains in the sample annealed at 100 °C (Figure 6c). The

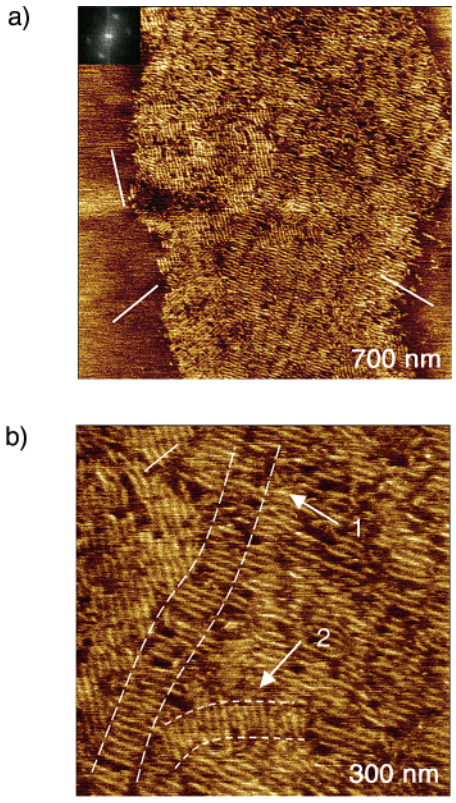

Figure 3. (a) AFM phase image of a large single-layer poly[(*3,4*−*3,5*)12G2−4EBn] domain obtained in hard tapping mode. White lines indicate directions along which the macromolecular rods are oriented. A power spectrum of FFT of the image is shown in the inset. (b) Magnification of a section of the domain shown in (a). White dotted lines define poly[(*3,4*−*3,5*)12G2−4EBn] lamella 1 and 2 inside this surface location.

macromolecular order of this domain can be described as the 2D nematic phase. A continuity of extended rods reflects the improvement of macromolecular ordering in this structural phase. Single extended rods, which exhibit a slightly twisted shape, appear as bright strips of ∼4 nm in width exceeding hundreds of nanometers in length. Darker regions between neighboring bright strips, which are ∼3.5−4 nm in width, most likely are related to a less dense polymer material (e.g., peripheral side chains). A quite similar situation is observed in the semicrystalline polymers such as poly(ethylene terephthalate), where a stack structure is formed by an alternation of lamellae cores and amorphous regions.[22]

The phase images in Figure 7 illustrate the variation of packing density within different domains in the same sample. In Figure 7a, the domains with the compact packing (∼7.2 nm) are neighboring a domain in which the spacing between the neighboring macromolecular rods is much larger (∼8.5 nm). At a surface location in Figure 7b one sees that the macromolecular rods can be oriented perpendicular to the HOPG step. A similar finding had been mentioned for dendronized poly(oxazoline)s.[14] White grains seen at the edges belong to the traces of the second layer.

Double Layers. The surface domains in Figures 2 and 3 exhibit a macromolecular order in the layer immediately lying on the substrate and a poor order structure of the top layer. We have examined poly[(*3,4*−*3,5*)12G2−4EBn] samples covered by a second layer to a larger extent (Figure 8). Figure 8a reveals the surface topography with some imperfections such as holes and small droplets. The top surface is characterized by grainy structure, which is most pronounced in the height images obtained in light tapping (Figure 8b). A step height measured at the holes is ∼1.7 nm. As shown below, this is the thickness of the double layers. Under the same conditions, the phase images are practically featureless. With increasing force, resolution of the grainy structures does not improve in the height image, but the step-height at the edge of the hole is substantially reduced (Figure 8e). The phase image recorded in hard tapping shows multiple macromolecular rods (Figure 8f). These changes are reversible; the grainy structure reappears when the tip force is reduced.

These observations are similar not only to those shown in Figure 4a,b, but also to many others on surfaces of polymer samples where a topmost layer is in a rubbery-like state. Such top layers can be easily pressed or penetrated by the probe, and it reveals an ordering of more rigid subsurface structures. Therefore, the pattern seen in the phase images by hard tapping described a macromolecular ordering in the poly[(*3,4*−*3,5*)-12G2−4EBn] layer lying on the HOPG (Figure 8f). The resolution of individual macromolecules and their lamellar order in this image is inferior to that in the images of single poly-[(*3,4*−*3,5*)12G2−4EBn] layer. This might be related to a partial involvement of grainy structures of the top layer to the image formation. Quantitative estimates of the rods forming the lamellar blocks in this image provide an average length of the rod ∼15 nm, which is smaller than the average length found in the images of single-layer structures. This result might be expected if we suggest that some parts of poly[(*3,4*−*3,5*)12G2−4EBn] macromolecules do not appear in the phase image of the double-layer aggregate. Incomplete penetration of the topmost layer may obscure portions of the macromolecules adsorbed to the HOPG surface despite using hard tapping. It also shows that a quantitative evaluation of the macromolecular dimensions from AFM images should be done with great care.

Direct confirmation about the double-layer nature of the poly-[(*3,4*−*3,5*)12G2−4EBn] adsorbate came from the following experiments (Figure 9). First, we have estimated the depth of the holes seen in the large-scale images. A location with one such hole is shown in Figure 9a,b. The cross-section profile, which was taken along the hole, shows that the adsorbate is formed of two layers each ∼0.8 nm in thickness (Figure 9c). The top layer shows grainy structures, whereas macromolecular rods are organized in the first layer. Traces of these rods are seen at the edges of the hole (especially in the phase image) and in some depressed surface locations on the right side of the hole. Second, we have checked the thickness and structure of the adsorbates by measuring vertical dimensions of a window scratched within the adsorbate by the AFM probe in the contact mode operation (see Experimental Section). A part of such a window is shown at the top of Figure 9d. A bearing analysis of the area marked by a box shows that the step height is ∼1.6 nm, consistent with the depth of the holes.

The AFM phase images recorded at the surface location where the double layer is neighboring the single layer are shown in Figure 10. The first image was obtained with a relatively low force. Therefore, one sees the top grainy structure of the double-layer region (top part of the image) and barely resolved individual rods of the single-layer region (bottom part of the image). With increased force, macromolecular lamellae and domains with extended rods of the first layer are seen in the top part of the image. The twisted macromolecular rods became distinctively seen in the bottom part of the image. Most likely, macromolecular ordering in the single poly[(*3,4*−*3,5*)12G2−4EBn] layer on HOPG proceeds differently when the layer is free or when it is confined by the top layer.

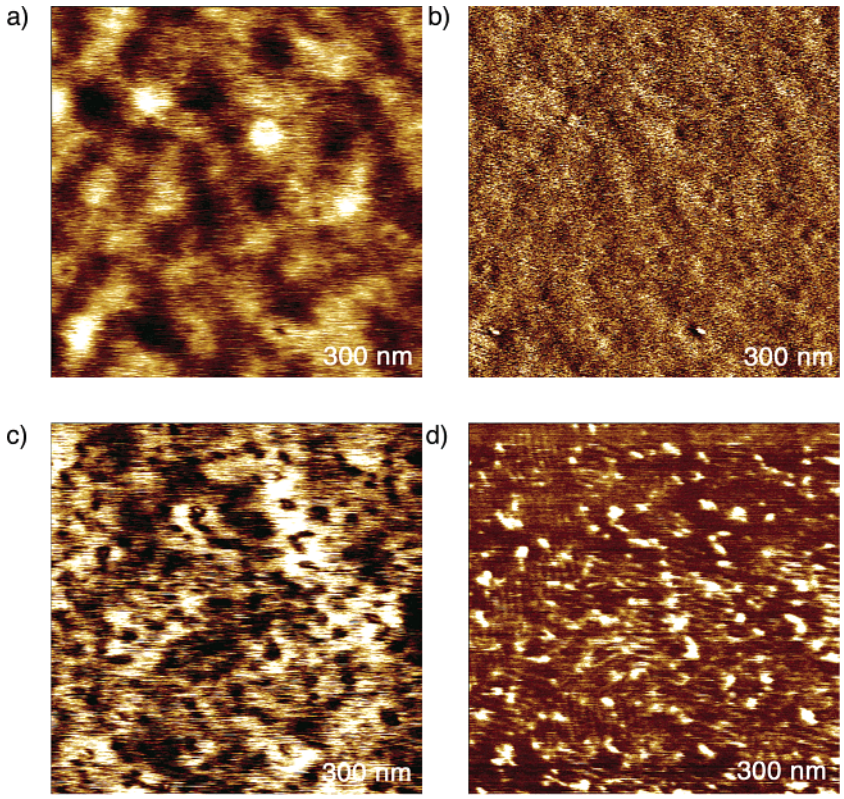

Figure 4. Effect of varying the tip−sample force to image individual poly[(*3,4*−*3,5*)12G2−4EBn] macromolecules from the domain shown in Figure 3a. (a, c) AFM height and (b, d) phase images obtained in (a, d) light tapping and (c, d) hard tapping modes.

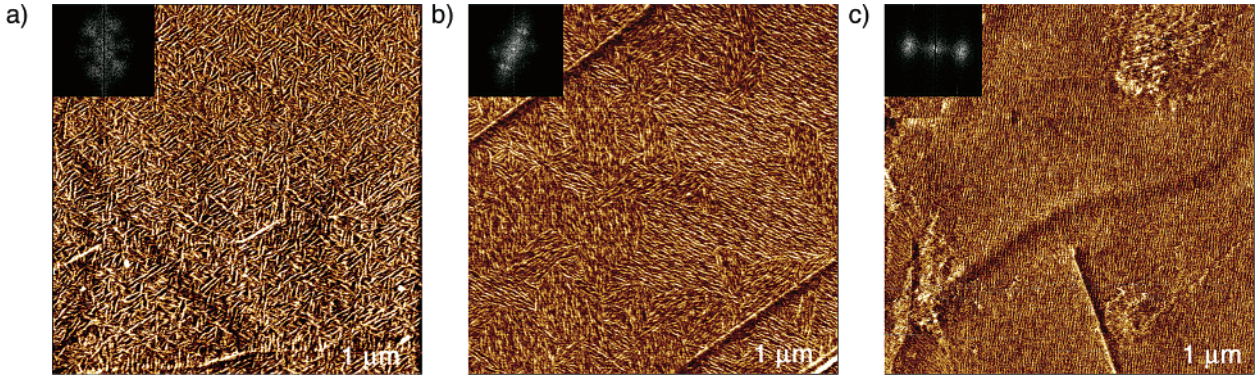

Figure 5. AFM phase image and power spectrum of FFT of the image (inset) of a single layer of poly[(*3,4*−*3,5*)12G2−4EBn] (a) spin-cast on HOPG and after annealing for 1 h at (b) 50 °C and (c) at 100 °C.

Discussion

Structural and retrostructural analysis of poly[(*3,4*−*3,5*)-12G2−4EBn] in bulk by a combination of DSC, XRD, electron density maps, and experimental density measurements revealed a thermoreversible cis−cisoidal to cis−transoidal conformational isomerization.[15a] Up to ∼90 °C the cylindrical dendronized PPA self-organizes into a Φ_h^{io} lattice. In the Φ_h^{io} lattice, the column diameter (D_{col}) is 4.69 nm (70 °C), and the column length per repeat unit (l_{XRD}) in the cis−cisoidal conformation is ∼0.14 nm. The helical and porous features of the Φ_h^{io} lattice are not observed in the Φ_h lattice at higher temperature. In the Φ_h lattice, where the PPA backbone adopts a cis−transoidal conformation, $D_{col} = 4.49$ nm and $l_{XRD} \sim 0.18$ nm.

We have confirmed the living character for polymerization of dendritic phenylacetylenes[15b] initiated by Rh(C≡CPh)(2,5-norbornadiene)$(PPh_3)_2$/4-(dimethylamino)pyridine (1:10).[23] As such, we can estimate the average length of the polymer chain based in the theoretical DP ($DP_{th} = [M]_0/[I]_0 = 52$) corrected for conversion (95%). This catalyst system has a low initiator efficiency (∼1/3), so the estimate should be based on $3 \times DP_{th} \times 0.95$. For the more compressed conformation found in the Φ_h^{io} phase the molecular length is ∼20.1 nm, and in the more extended Φ_h phase it is ∼27.5 nm.

We found out that imaging of the poly[(*3,4*−*3,5*)12G2−4EBn] single layers was quite unusual. In such cases, AFM images, which have revealed poly[(*3,4*−*3,5*)12G2−4EBn] macromolecules, were obtained only when an initial amplitude of a free-oscillating probe $A_0 = 60-80$ nm has dropped to a set-point value $A_{sp} = 2-3$ nm. In other words, a largest part of the probe oscillation was damped within a soft nonordered layer, which according to our estimates was ∼40 nm.[25] Thermal annealing of the poly[(*3,4*−*3,5*)12G2−4EBn] samples at 100 °C did not substantially reduce the thickness of this layer. We suggest that this layer had been formed due to a partial

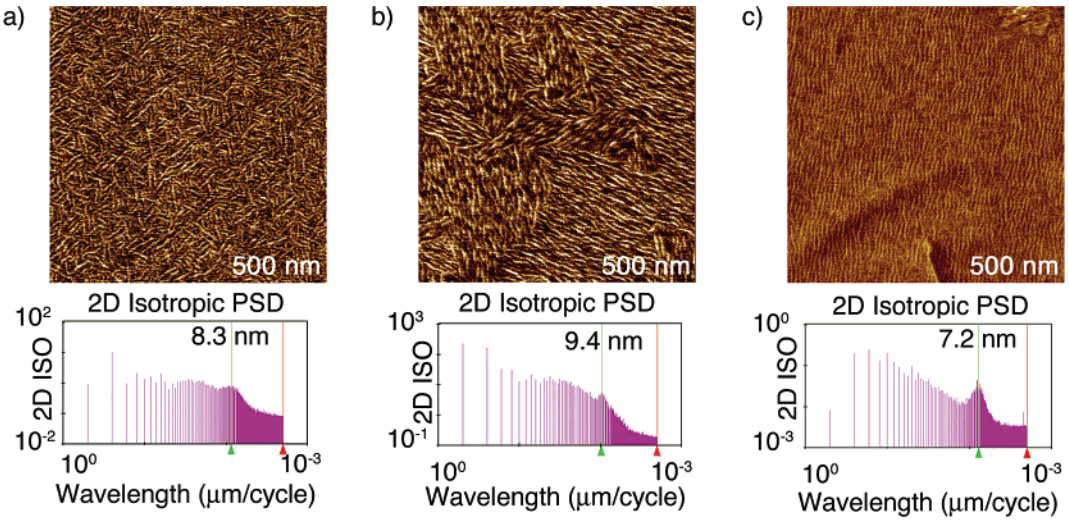

Figure 6. High-resolution AFM phase image of a single layer of poly[(*3,4*−*3,5*)12G2−4EBn] (a) spin-cast on HOPG and after annealing for 1 h at (b) 50 °C and (c) at 100 °C. Power spectrum density for each of these images is shown underneath.

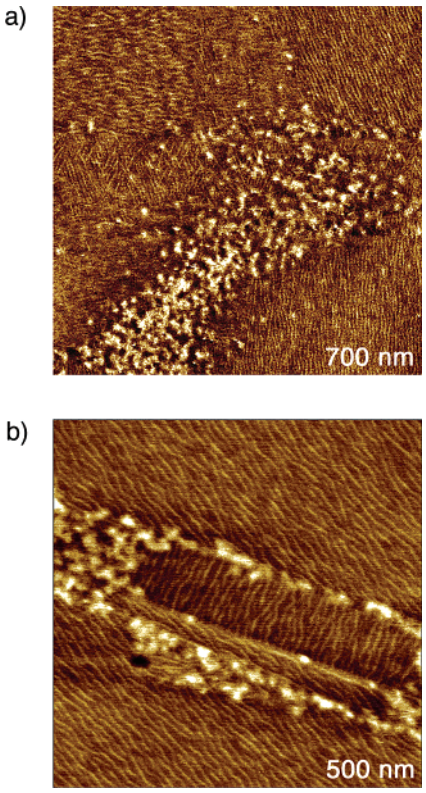

Figure 7. Phase images of different locations of the single layer of poly[(*3,4*−*3,5*)12G2−4EBn] after annealing at 100 °C.

incorporation of solvent molecules into the polymer. In the study of double-layer adsorbates, we have applied imaging at different force levels (light tapping and hard tapping[25]) in order to reveal the structure of the underlying layer. In such cases a tip-induced deformation of the top layer was in the nanometer range and hard tapping with $A_{sp} \sim 0.5A_0$ allowed high-resolution imaging of the polymer layer lying immediately on the substrate.

Comparison of these estimates to the experimentally found molecular lengths in macromolecular arrays and single and double layers can serve as a starting point to understand the observed self-assembly processes. In molecular arrays at the HOPG surface, we imaged species whose typical length is ∼23 nm. This is within the estimated range and suggests that the polymer adopts a more extended conformation than in the compact Φ_h^{io} phase. Epitaxial adsorption of the peripheral alkyl tails to the HOPG surface leads to more extended polymer conformations.

In the double-layer adsorbates the molecular length in the layer adsorbed to the HOPG surface was found to be ∼15 nm. Underestimation of the molecular length is likely because the measurement is made in hard tapping mode. Nonetheless, macromolecules in the second layer likely adopt a more compact conformation. The polymer conformation is not as significantly determined by the HOPG surface and may be more similar to that proposed for the Φ_h^{io} phase. Nonetheless, the directional orientation of the molecules is enforced by the symmetry of the underlying HOPG.

In the single-layer adsorbate, ordering due to epitaxy is observed in the as-prepared sample, while intercolumnar interactions appear to be absent. Thermal annealing at 50 and 100 °C demonstrates self-organization that is driven by strong intercolumnar interactions, including end-to-end self-assembly:[14] improved 2D nematic ordering of the cylindrical dendronized PPAs. It is interesting to compare these dendronized PPAs to poly(oxazoline)s (DP = 100) jacketed with self-assembling minidendrons.[14] In single layers, the molecules appear to be of comparable length ∼23 nm. Recently, it was rationalized that the tendency of short (∼15−40 nm) poly(phthalocyanatosiloxane) macromolecules to form elongated assemblies on HOPG results from a head-to-tail motif[24] similar to the dendronized poly(oxazoline)s.[14] An apparent driving force for the formation of significantly longer head-to-tail assemblies of short cylindrical macromolecules is the relative surface area associated with chain ends compared to the overall macromolecule. An additional contribution may come from the more dynamic behavior of the smaller polymers (i.e., fewer points of contact with the surface). Since an isotropic liquid phase is not observed for poly[(*3,4*−*3,5*)12G2−4EBn], intercolumnar interactions are expected to dominate the annealing process.

We have recently shown several examples of self-organizable dendronized PPAs whose column diameters determined in bulk by XRD are similar to the width measured by AFM of the macromolecule on HOPG or mica.[15b] Rationale for the discrepancy observed between AFM on HOPG and XRD in bulk was provided in terms of a more oblate macromolecular object (Scheme 2) due to epitaxy of the peripheral alkyl tails. A more detailed discussion of this is valuable in the current context.

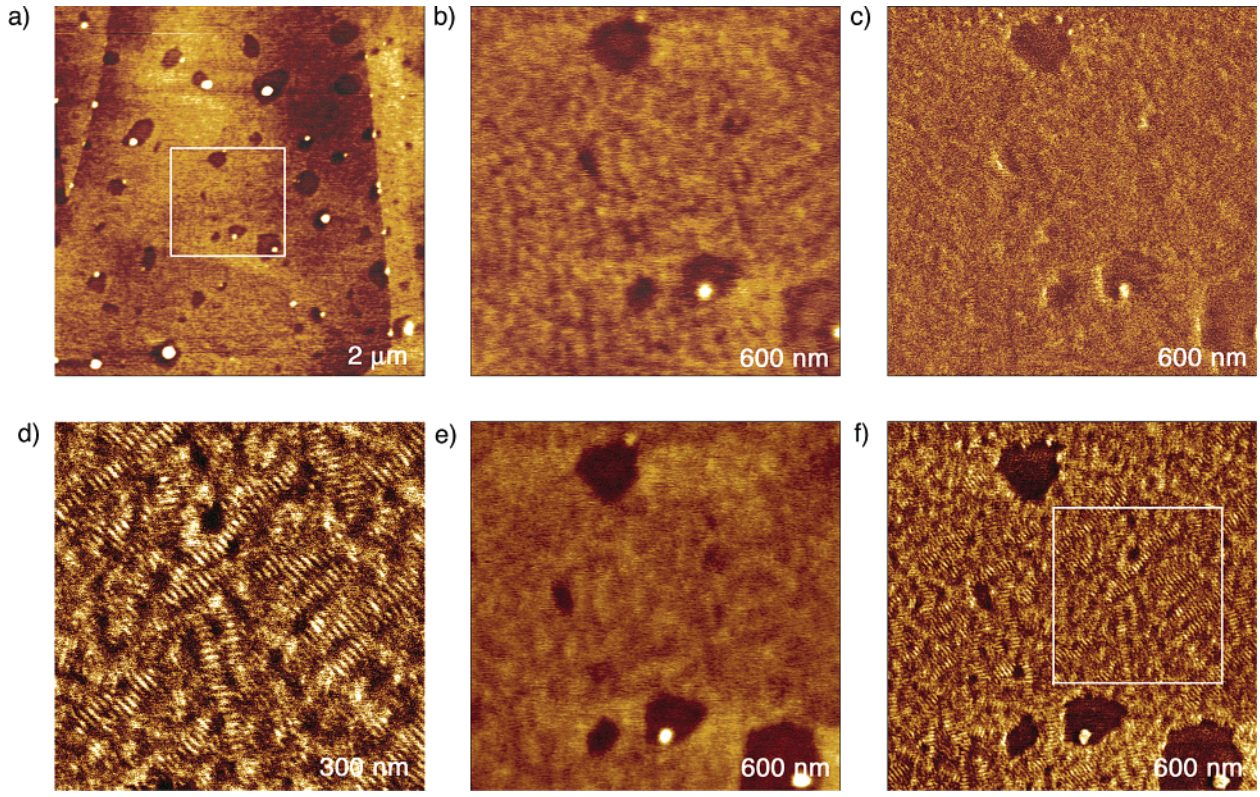

Figure 8. (a) AFM height image of a double layer of poly[(*3,4*−*3,5*)12G2−4EBn] on HOPG. (b) Height and (c) phase images of one of the locations in (a) obtained in light tapping. (e) Height and (f) phase images of the same location as in (b) and (c) obtained in hard tapping. (d) High-resolution phase image of a part of the area shown in (e) and (f).

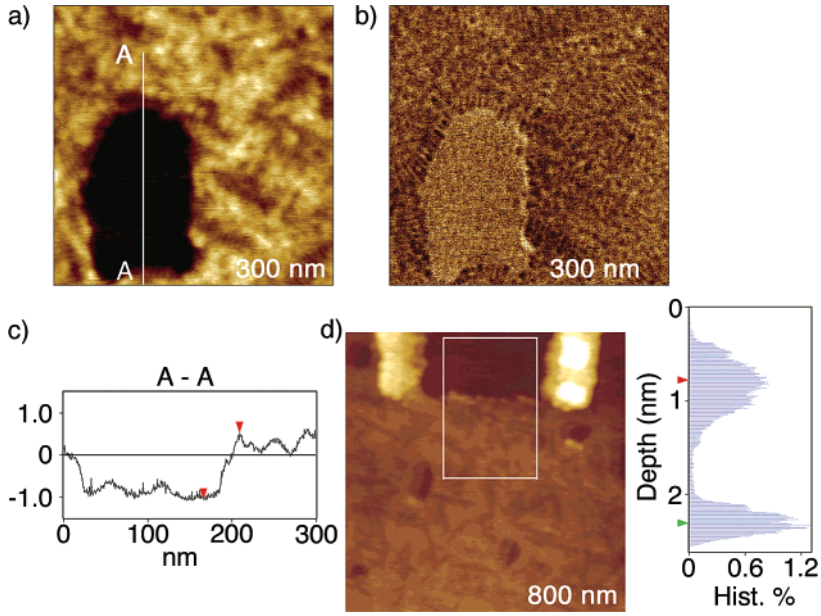

Figure 9. (a) Height and (b) phase images of a double layer of poly[(*3,4*−*3,5*)12G2−4EBn]. (c) A cross-section profile, which is taken along the line A−A in (a). (d) Height image of a double-layer region, which includes part of a window obtained by scratching with the AFM probe. A bearing analysis histogram of a region indicated with a black box in the image is shown on the right side.

Both in macromolecular arrays and in single layers, the average height of a layer is ∼0.7 nm. This thickness appears to be quantized upon examination of the double layer whose thickness is ∼1.7 nm. The uniformity of this layer suggests that it is comprised of a single, well-defined species. We ascribe this behavior to adsorption of single cylindrical PPAs rather than their aggregates.

For this to be true, we expect to find periodicity within the layer that is consistent with the column diameter determined in bulk by XRD. The average width of the bright objects visualized in macromolecular arrays is ∼4 nm and ∼4−5 nm in the single layer. The dark region between neighboring objects adds ∼3.5−4 nm to each cylindrical object. This accounts for the softer alkyl tail periphery and results in an average width that is larger by AFM than the diameter measured by XRD. Dendronized PPAs in the Φ_h (or Φ_h^{io}) phase are treated as uniform circular shapes, but on the HOPG surface the height and width are different. We can consider the cross-sectional

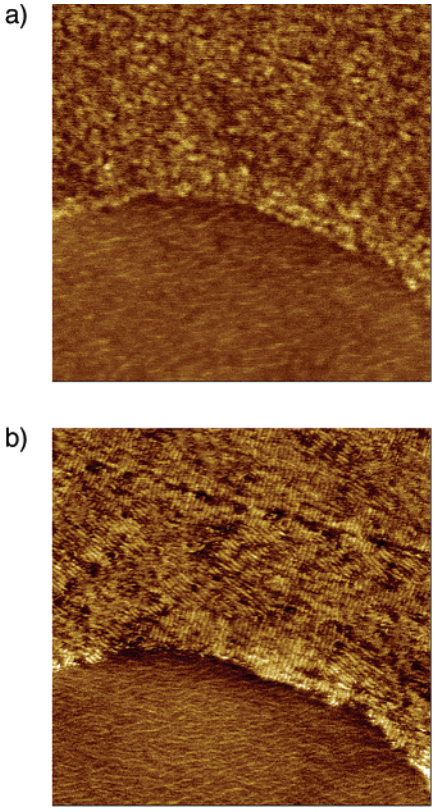

Figure 10. Phase images obtained in (a) light tapping and (b) hard tapping modes of a location of poly[(*3,4*−*3,5*)12G2−4EBn] adsorbate with a double-layer region on the top and a single-layer region at the bottom.

Scheme 2

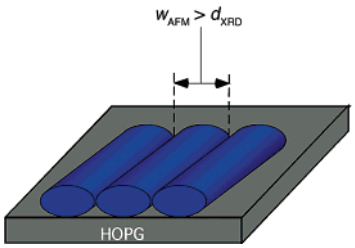

area of a single object from each method. From XRD at 70 and 105 °C the cross-sectional areas are 19 and 16 nm^2, respectively. Using the average width of 8 nm, we calculate a cross-sectional area of 18 nm^2 from AFM. Again, this is consistent with the dimensions expected for an individual cylindrical dendronized PPA.

The oblate shape of cylindrical self-organizable dendronized polymers observed by AFM on HOPG results from maximizing the number of epitaxial contacts. A more circular shape increases the vertical dimension of the object and reduces the number of chains capable of participating in epitaxy. Peripheral alkyl chains epitaxially adsorbed to the HOPG surface adopt a fully extended conformation and occupy a corresponding volume, which prevents adsorption of some neighboring chains on the same macromolecule. The widths of macromolecules observed in as-prepared samples range from ∼7.2 to ∼8.5 nm. This variance reflects kinetic entrapment of less dense cylindrical packing arrangements during spin-casting. Large domains of ∼7.2 nm cylindrical PPAs found after thermal annealing indicate that this dimension reflects a thermodynamically densest packing. A closer approach of cylindrical poly[(*3,4*−*3,5*)12G2−4EBn] macromolecules requires a more circular shape (i.e., fewer epitaxial contacts) or results in competition for HOPG surface area by epitaxially adsorbed alkyl chains between adjacent macromolecules.

Conclusions

Poly[(*3,4*−*3,5*)12G2−4EBn] is visualized by AFM on HOPG as oblate cylindrical objects whose relative orientation in the first layer adsorbed to the HOPG reflects underlying lattice symmetry. Comparison of the height and width profiles from AFM images with the column diameter measured in XRD experiments confirms that the objects are individual macromolecules. The oblate shape and orientation of the cylindrical PPA is attributed to epitaxial adsorption of the peripheral alkyl tails. Thermal annealing in the Φ_h^{io} and Φ_h phases results in large domains 2D nematic order due to intermolecular interactions. The dimensions of the oblate cylindrical PPA dictate the periodicity within domains and between layers. The increase sample thickness upon going from single to double layers is quantized. Domains with different packing density are observed. The macromolecular length on the HOPG surface is larger than that expected for poly[(*3,4*−*3,5*)12G2−4EBn] based on a model for a helical cis−cisoidal PPA backbone in the Φ_h^{io} phase.[15a] This indicates a more extended backbone conformation and arises from epitaxial adsorption of the peripheral alkyl chains on the HOPG surface.

Experimental Section

Polymer Synthesis and Characterization. Using Rh(C≡CPh)(2,5-norbornadiene)$(PPh_3)_2$/4-(dimethylamino)pyridine (1:10),[23] poly[(*3,4*−*3,5*)12G2−4EBn] was prepared from the corresponding macromonomer. Details of the synthesis and characterization have been reported elsewhere.[15] The sample examined herein was found to have M_n = 61 300 and M_w/M_n = 1.22 by GPC in THF (1 mL/min) calibrated with polystyrene standards. The cis content was determined by ^{1}H NMR (500 MHz) spectroscopy according to a method previously developed in our group.[21a,b] By this method the cis content for poly[(*3,4*−*3,5*)12G2−4EBn] we found to be 87%.[15a] Although we have provided a method that accounts for the presence of cyclohexadiene moieties,[21c,d] this could not be applied to dendronized PPAs due to overlapping resonances.[15]

Sample Preparation. Sample preparation was made using spin-casting, in which a droplet of diluted solution of poly[(*3,4*−*3,5*)-12G2−4EBn] (0.002−0.01 mg/mL) in THF was deposited on a freshly cleaved surface of HOPG. It is worth noting that a preparation of single polymer layers on a HOPG substrate requires multiple trials. Among the factors influencing this preparation is the presence of surface defects such as graphite steps at which more concentrated patches of materials are formed during spin-casting, drying, and annealing. Most of thermal annealing was performed in a vacuum oven at 100 °C.

AFM Measurements. AFM Experiments were carried out with a scanning probe microscope MultiMode Nanoscope IIIa (Digital Instruments/Veeco Metrology Group) equipped with a scanner, which allows imaging surface areas larger than 100 μm. For some experiments, which required sample annealing, we have used a commercial thermal accessory of the MultiMode microscope. The sample was annealed at elevated temperatures yet all AFM measurements were performed at ambient conditions. Tapping mode was used in most experiments. The contact AFM mode was applied only for a scratching of a window within an adsorbate layer. This procedure is applied for estimation of a thickness of an adsorbate layer. After the scratching, a surface area including the window was imaged in tapping mode. A step height at the window border defines the layer thickness.

In our tapping mode AFM studies, we simultaneously recorded height and phase images. When tip−sample force interactions are minimized, the height images reproduce surface topography. With an increase of the tip force, a surface deformation might show up

in the height images. The phase images, in which a contrast reflects a difference of the phases of free-oscillating and interacting probes, depend on imaging conditions even more strongly than the height images. Depending on the tip−sample force level, the phase contrast might enhance fine details of the surface topography or might emphasize individual components of heterogeneous polymer systems.[25] In studies of single macromolecules, images of both kinds are quite useful.

There are two important issues with the AFM imaging of single poly[(*3,5*−*3,5*)12G2−4EBn] macromolecules and assemblies. One relates to the choice of operation conditions (i.e., the level of tip−sample force interactions). The top of the polymer adsorbate on HOPG might consist of a poorly ordered material, and the AFM probe should penetrate this overlayer to come into contact with rigid and ordered structures lying on the substrate.[14] The analysis of the operation conditions will be incomplete without a description of the probes. Noncoated Si etched probes (length ∼225 μm, width ∼40 μm) with different stiffness (1−3 N/m, resonance frequency 50−60 kHz, and 40−50 N/m, resonance frequency 150−170 kHz) were applied in our measurements. In cases when imaging with the stiffer probes has induced sample damage, the same sample was reexamined with the softer probes. When the latter probes were not strong enough to penetrate through top surface layers, imaging was performed at the higher resonance frequency of these probes (∼300−360 kHz) or the stiffer probes were applied. The amplitude of the probe before engagement (A_0) was typically 40−50 nm, and the set-point amplitude (A_{sp}) varies from values close to A_0 (light tapping) to 20−30 nm (hard tapping). In some cases smaller A_{sp} were applied to allow the probe to reach structures underneath the soft top layer.

The second issue we would like to mention is related to a calibration of AFM piezo-scanners, which define an accuracy of the submicron measurements. The piezo-ceramic, which is used for such scanners, exhibits nonlinearity, creep, and other imperfections common to polycrystalline materials. A so-called J-scanner, which we have applied in our measurements, allows scanning of large surface areas (above 100 μm on side). The capability of large scans is always desirable when surface regions are expected to be heterogeneous as in the case of the samples we have examined. The J-scanners are typically calibrated with a standard grating having 1 μm × 1 μm patterns (in lateral, *x*- and *y*-directions) and steps of 180 nm (in vertical, *z*-direction). Definitely, such calibration is not sufficient when this scanner is applied for visualization of objects in the sub-100 nm range. To make necessary adjustments in the calibration parameters of the J-scanner, we have used this scanner for the contact mode imaging of the *ab*-plane of organic charge-transfer salt crystal of TTF−TCNQ (TTF = tetrathiafulvalene, TCNQ = tetracyanoquinodimethane), which has the following crystallographic parameters: $a = 1.2298$ nm, $b = 0.3819$ nm, $c = 1.8468$ nm, $\alpha = \gamma = 90°$, $\beta = 104.46°$.[26] So imaging of atomic-scale lattices with the J-scanner does not provide well-resolved patterns, a linear structure with a periodicity of 1.3 nm was clearly observed, and thus we obtained a ∼1.3/1.23 adjustment coefficient for lateral measurements, which is approximately the same for both *x*- and *y*-directions. To make adjustments in the *z*-calibration, we have measured surface steps, which according to the crystallographic data should be multiple of $0.5(c \cos 14.5°) = 0.895$ nm. A deviation of the *z*-calibration was within 10%, and it was corrected appropriately.

Acknowledgment. Financial support by the National Science Foundation (DMR-01-02459 and DMR-05-48559) is gratefully acknowledged.

References and Notes

(1) (a) Mamdouh, W.; Uji-i, H.; Ladislaw, J. S.; Dulcey, A. E.; Percec, V.; De Schryver, F. C.; De Feyter, S. *J. Am. Chem. Soc.* **2006**, *128*, 317−325. (b) Mamdouh, W.; Uji-i, H.; Dulcey, A. E.; Percec, V.; De Feyter, S.; De Schryver, F. C. *Langmuir* **2004**, *20*, 7678−7685. (c) De Feyter, S.; De Schryver, F. C. *Chem. Soc. Rev.* **2003**, *32*, 139−150. (d) De Feyter, S.; Gesquière, A.; Abdel-Mottaleb, M. M.; Grim, P. C. M.; De Schryver, F. C.; Meiners, C.; Sieffert, M.; Valiyaveettil, S.; Müllen, K. *Acc. Chem. Res.* **2000**, *33*, 520−531. (e) Lei, S. B.; Wang, C.; Yin, S. X.; Wang, N. H.; Xi., F.; Liu, H. W.; Xu, B.; Wan, L. J.; Bai, C. L. *J. Phys. Chem. B* **2001**, *105*, 10838−10841. (f) Giancarlo, L. C.; Flynn, G. W. *Acc. Chem. Res.* **2000**, *33*, 491−501. (g) Semenov, A.; Spatz, J. P.; Möller, M.; Lehn, J.-M.; Sell, B.; Schubert, D.; Weidl, C. H.; Schubert, U. S. *Angew. Chem.* **1999**, *111*, 2701−2705; *Angew. Chem., Int. Ed.* **1999**, *38*, 2547−2550. (h) Schlüter, A. D.; Rabe, J. P. *Angew. Chem.* **2000**, *112*, 869−880; *Angew. Chem., Int. Ed.* **2000**, *39*, 864−883. (i) Lee, C. C.; MacKay, J. A.; Fréchet, J. M. J.; Szoka, F. C. *Nat. Biotechnol.* **2005**, *23*, 1517−1526.

(2) (a) Binnig, G.; Rohrer, H.; Gerber, C.; Weibel, E. *Physica B & C* **1982**, *109 & 110*, 2075−2077. (b) Binnig, G.; Quate, C. F.; Gerber, C. *Phys. Rev. Lett.* **1986**, *56*, 930−933. (c) Colton, R. J.; Engel, A.; Frommer, J. E.; Gaub, H. E.; Gewrith, A. A.; Guckenberger, R.; Rabe, J.; Heckl, W. M.; Parkinson, B. *Procedures in Scanning Probe Microscopies*; J. Wiley & Sons: New York, 1998.

(3) (a) Magonov, S. N.; Whangbo, M.-H. *Surface Analysis with STM and AFM;* VCH Publishers: Weinheim, 1996. (b) Sheiko, S. S. *Adv. Polym. Sci.* **2000**, *151*, 61−174. (c) Sheiko, S. S.; Möller, M. *Chem. Rev.* **2001**, *101*, 4099−4123.

(4) Foster, J. S.; Frommer, J. E. *Nature (London)* **1988**, *333*, 542−545.

(5) McGonigal, G. C.; Bernhardt, R. H.; Thomson, D. J. *Appl. Phys. Lett.* **1990**, *57*, 28.

(6) Liang, W.; Whangbo, M.-H.; Wawkuschewski, A.; Cantow, H.-J.; Magonov, S. N. *Adv. Mater.* **1993**, *5*, 817−821.

(7) Groszek, A. *Proc. R. Soc. London* **1970**, *A314*, 473−498.

(8) (a) Wawkuschewski, A.; Cantow, H.-J.; Magonov, S. N.; Möller, M.; Liang, W.; Whangbo, M.-H. *Adv. Mater.* **1993**, *5*, 821−826. (b) Rabe, J. P.; Buchholz, S. *Science* **1991**, *253*, 424−427.

(9) Herwig, K. W.; Matthies, B.; Taub, H. *Phys. Rev. Lett.* **1995**, *75*, 3154−3157.

(10) Kumaki, J.; Nishikawa, Y.; Hashimoto, T. *J. Am. Chem. Soc.* **1996**, *118*, 3321−3322.

(11) (a) Frey, H.; Lach, C.; Lorenz, K. *Adv. Mater.* **1998**, *10*, 279−293. (b) Ponomarenko, S. A.; Boiko, N. I.; Zhu, H.-M.; Agina, E. V.; Shibaev, V. P.; Magonov, S. N. *Polym. Sci., Ser. C* **2001**, *43*, 245−257. (c) Ponomarenko, S. A.; Boiko, N. I.; Shibaev, V. P. *Langmuir* **2000**, *16*, 5487−5493. (d) Percec, V.; Dulcey, A. E.; Balagurusamy, V. S. K.; Miura, Y.; Smidrkal, J.; Peterca, M.; Nummelin, S.; Edlund, U.; Hudson, S. D.; Heiney, P. A.; Duan, H.; Magonov, S. N.; Vinogradov, S. A. *Nature (London)* **2004**, *430*, 764−768. (e) Percec, V.; Cho, W.-D.; Möller, M.; Prokhorova, S. A.; Ungar, G.; Yeardley, D. J. P. *J. Am. Chem. Soc.* **2000**, *122*, 4249−4250.

(12) Gerle, M.; Fischer, K.; Roos, S.; Müller, A. H. E.; Schmidt, M.; Sheiko, S. S.; Prokhorova, S.; Möller, M. *Macromolecules* **1999**, *32*, 2629−2637.

(13) (a) Percec, V.; Anh, C.-H.; Ungar, G.; Yeardley, D. J. P.; Möller, M.; Sheiko, S. S. *Nature (London)* **1998**, *391*, 161−164. (b) Prokhorova, S. A.; Sheiko, S. S.; Möller, M.; Anh, C.-H.; Percec, V. *Macromol. Rapid Commun.* **1998**, *19*, 359−366. (c) Percec, V.; Anh, C.-H.; Cho, W.-D.; Jamieson, A. M.; Kim, J.; Leman, T.; Schmidt, M.; Gerle, M.; Möller, M.; Prokhorova, S. A.; Sheiko, S. S.; Cheng, S. Z. D.; Zhang, A.; Ungar, G.; Yeardley, D. J. P. *J. Am. Chem. Soc.* **1998**, *120*, 8619−8631. (d) Prokhorova, S. A.; Sheiko, S. S.; Anh, C.-H.; Percec, V.; Möller, M. *Macromolecules* **1999**, *32*, 2653−2660. (e) Prokhorova, S. A.; Sheiko, S. S.; Mourran, A.; Azumi, R.; Beginn, U.; Zipp, G.; Anh, C.-H.; Holerca, M. N.; Percec, V.; Möller, M. *Langmuir* **2000**, *16*, 6862−6867.

(14) Percec, V.; Holerca, M. N.; Magonov, S. N.; Yeardley, D. J. P.; Ungar, G.; Duan, H.; Hudson, S. D. *Biomacromolecules* **2001**, *2*, 706−728.

(15) (a) Percec, V.; Rudick, J. G.; Peterca, M.; Wagner, M.; Obata, M.; Mitchell, C. M.; Cho, W.-D.; Balagurusamy, V. S. K.; Heiney, P. A. *J. Am. Chem. Soc.* **2005**, *127*, 15257−15264. (b) Percec, V.; Rudick, J. G.; Peterca, M.; Staley, S. R.; Wagner, M.; Obata, M.; Mitchell, C. M.; Cho, W.-D.; Balagurusamy, V. S. K.; Lowe, J. N.; Glodde, M.; Weichold, O.; Chung, K. J.; Ghionni, N.; Magonov, S. N.; Heiney, P. A. *Chem.*−*Eur. J.* **2006**, *12*, 5731−5746.

(16) (a) Stocker, W.; Karakaya, B.; Schürmann, B. L.; Rabe, J. P.; Schlüter, A. D. *J. Am. Chem. Soc.* **1998**, *120*, 7691−7695. (b) Stocker, W.; Schürmann, B. L.; Rabe, J. P.; Förster, S.; Lindner, P.; Neubert, I.; Schlüter, A.-D. *Adv. Mater.* **1998**, *10*, 793−797. (c) Shu, L.; Gössl, I.; Rabe, J. P.; Schlüter, A. D. *Macromol. Chem. Phys.* **2002**, *203*, 2540−2550. (d) Ecker, C.; Severin, N.; Shu, L.; Schlüter, A. D.; Rabe, J. P. *Macromolecules* **2004**, *37*, 2484−2489. (e) Shu, L.; Schlüter, A. D.; Ecker, C.; Severin, N.; Rabe, J. P. *Angew. Chem.* **2001**, *113*, 4802−4805; *Angew. Chem., Int. Ed.* **2001**, *40*, 4666−4669. (f) Gössl, I.; Shu, L.; Schlüter, A. D.; Rabe, J. P. *J. Am. Chem. Soc.* **2002**, *124*, 6860−6865.

(17) (a) Lee, C. C.; Fréchet, J. M. J. *Macromolecules* **2006**, *39*, 476−481. (b) Yoshida, M.; Fresco, Z. M.; Ohnishi, S.; Fréchet, J. M. J. *Macromolecules* **2005**, *38*, 334−344.

(18) Percec, V.; Anh, C.-H.; Barboiu, B. *J. Am. Chem. Soc.* **1997**, *119*, 12978−12979.
(19) (a) Nakano, T.; Okamoto, Y. *Chem. Rev.* **2001**, *101*, 4013−4038. (b) Yashima, E.; Maeda, K.; Nishimura, T. *Chem.*—*Eur. J.* **2004**, *10*, 42−51.
(20) (a) Shinohara, K.-I.; Yasuda, S.; Kato, G.; Fujita, M.; Shigekawa, H. *J. Am. Chem. Soc.* **2001**, *123*, 3619−3620. (b) Shinohara, K.-i.; Kitami, T.; Nakamae, K. *J. Polym. Sci., Part A: Polym. Chem.* **2004**, *42*, 3930−3935. (c) Nishimura, T.; Takatani, K.; Sakurai, S.-i.; Maeda, K.; Yashima, E. *Angew. Chem.* **2002**, *114*, 3754−3756; *Angew. Chem., Int. Ed.* **2002**, *41*, 3602−3604. (d) Sakurai, S.-i.; Kuroyanagi, K.; Morino, K.; Kunitake, M.; Yashima, E. *Macromolecules* **2003**, *36*, 9670−9674. (e) Nishimura, T.; Tsuchiya, K.; Ohsawa, S.; Maeda, K.; Yashima, E.; Nakamura, Y.; Nishimura, J. *J. Am. Chem. Soc.* **2004**, *126*, 11711−11717. (f) Sakurai, S.-i.; Kuroyanagi, K.; Nonokawa, R.; Yashima, E. *J. Polym. Sci., Part A: Polym. Chem.* **2004**, *42*, 5838−5844. (g) Sakurai, S.-i.; Ohira, A.; Suzuki, Y.; Fujito, R.; Nishimura, T.; Kunitake, M.; Yashima, E. *J. Polym. Sci., Part A: Polym. Chem.* **2004**, *42*, 4621−4640. (h) Maeda, K.; Ishikawa, M.; Yashima, E. *J. Am. Chem. Soc.* **2005**, *126*, 15161−15166. (i) Sakurai, S.-i.; Okoshi, K.; Kumaki, J.; Yashima, E. *Angew. Chem.* **2006**, *118*, 1267−1279; *Angew. Chem., Int. Ed.* **2006**, *45*, 1245−1248. (j) Li, B. S.; Cheuk, K. K. L.; Salhi, F.; Lam, J. W. Y.; Cha, J. A. K.; Xiao, X.; Bai, C.; Tang, B. Z. *Nano Lett.* **2001**, *1*, 323−328. (k) Li, B. S.; Cheuk, K. K. L.; Ling, L.; Chen, J.; Xiao, X.; Bai, C.; Tang, B. Z. *Macromolecules* **2003**, *36*, 77−85.
(21) (a) Simionescu, C. I.; Percec, V.; Dumitrescu, S. *J. Polym. Sci., Polym. Chem.* **1977**, *15*, 2497−2509. (b) Simionescu, C. I.; Percec, V. *J. Polym. Sci., Polym. Lett. Ed.* **1979**, *17*, 421−429. (c) Percec, V. *Polym. Bull. (Berlin)* **1983**, *10*, 1−7. (d) Percec, V.; Rudick, J. G. *Macromolecules* **2005**, *38*, 7241−7250.
(22) Ivanov, D. A.; Amalou, Z.; Magonov, S. N. *Macromolecules* **2001**, *34*, 8944−8952.
(23) (a) Kishimoto, Y.; Eckerle, P.; Miyatake, T.; Ikariya, T.; Noyori, R. *J. Am. Chem. Soc.* **1994**, *116*, 12131−12132. (b) Kishimoto, Y.; Eckerle, P.; Miyatake, T.; Kainosho, M.; Ono, A.; Ikariya, T.; Noyori, R. *J. Am. Chem. Soc.* **1999**, *121*, 12035−12044.
(24) Samorí, P.; Engelkamp, H.; de Witte, P. A. J.; Rowan, A. E.; Nolte, R. J. M.; Rabe, J. P. *Adv. Mater.* **2005**, *17*, 1265−1268.
(25) Magonov, S. N. Visualization of Polymers at Surfaces and Interfaces. In *Handbook of Surfaces of Materials*; Singh, N. H., Ed.; Academic Press: New York, 2001; Vol. 2.
(26) Kistenmacher, T. J.; Philips, T. E.; Cowan, D. O. *Acta Crystallogr. B* **1974**, *30*, 763.

MA060845G